Investigation of FWM in dispersion-engineered GaInP photonic crystal waveguides

Kevin Lenglé, Laurent Bramerie, Mathilde Gay, Marcia Costa E Silva, Sebastien Lobo, Jean-Claude Simon, Pierre Colman, Sylvain Combrié, Alfredo de Rossi

Investigation of FWM in dispersion-engineered GaInP photonic crystal waveguides

Kevin Lengle,[1,2,*] Laurent Bramerie,[1,2] Mathilde Gay,[1,2] Marcia Costa e Silva,[1,2] Sebastien Lobo,[1,2] Jean-Claude Simon,[1,2] Pierre Colman,[3] Sylvain Combrie,[3] and Alfredo de Rossi[3]

[1]*Université européenne de Bretagne, 5 Boulevard Laënnec, 35000 Rennes, France*
[2]*CNRS Foton (UMR 6082), BP 80518, 22305 Lannion cedex, France*
[3]*Thales Research and Technology, 1 Avenue A.Fresnel, 91767 Palaiseau, France*
[*]*lengle@enssat.fr*

Abstract: We report on the investigation of four-wave mixing (FWM) in a long (1.3 mm) dispersion-engineered Gallium Indium Phosphide (GaInP) photonic crystal (PhC) waveguide. A comparison with a non-engineered design is made with respect to measured FWM efficiency maps. A striking different response is observed, in terms of dependence on the pump wavelength and the spectral detuning. The benefits and the limitations of both structures are discussed, in particular the trade-off between slow-light enhancement of the FWM efficiency and the conversion bandwidth. The time-resolved parametric conversion of short pulses at 10 GHz is also shown. Finally, the transmission capability of a 40 Gbit/s RZ signal is assessed through bit-error rate measurements, revealing error-free operation with only 1dB penalty.

OCIS codes: (130.5296) Photonic crystal waveguides; (190.3270) Kerr effect; (190.4380) Nonlinear optics, four-wave mixing.

References and links

1. P. Colman, C. Husko, S. Combrié, I. Sagnes, C. W. Wong, and A. De Rossi, "Observation of soliton pulse compression in photonic crystal waveguides," in *Quantum Electronics and Laser Science Conference*, OSA Technical Digest (CD) (Optical Society of America, 2010), paper QPDA10.
2. J. T. Mok and B. J. Eggleton, "Photonics: expect more delays," Nature **433**(7028), 811–812 (2005).
3. A. Shinya, S. Matsuo, T. Yosia, E. Tanabe, T. Kuramochi, T. Sato, Kakitsuka, and M. Notomi, "All-optical on-chip bit memory based on ultra high Q InGaAsP photonic crystal," Opt. Express **16**(23), 19382–19387 (2008).
4. K. Nozaki, T. Tanabe, A. Shinya, S. Matsuo, T. Sato, H. Taniyama, and M. Notomi, "Sub-femtojoule all-optical switching using a photonic-crystal nanocavity," Nat. Photonics **4**(7), 477–483 (2010).
5. J. Leuthold, C. Koos, and W. Freude, "Nonlinear silicon photonics," Nat. Photonics **4**(8), 535–544 (2010).
6. J. Li, L. O'Faolain, I. H. Rey, and T. F. Krauss, "Four-wave mixing in photonic crystal waveguides: slow light enhancement and limitations," Opt. Express **19**(5), 4458–4463 (2011).
7. C. Monat, M. Ebnali-Heidari, C. Grillet, B. Corcoran, B. J. Eggleton, T. P. White, L. O'Faolain, J. Li, and T. F. Krauss, "Four-wave mixing in slow light engineered silicon photonic crystal waveguides," Opt. Express **18**(22), 22915–22927 (2010).
8. S. Combrié, P. Colman, C. Husko, Q. V. Tran, and A. De Rossi, "Advances in III-V based photonic crystals for integrated optical processing," Proc. SPIE **7608**, 760815 (2010).
9. H. Benisty, J. M. Lourtioz, A. Chelnokov, S. Combrie, and X. Checoury, "Recent Advances toward optical devices in semiconductor based photonic crystals," Proc. IEEE **94**(5), 997–1023 (2006).
10. T. Baba, "Slow light in photonic crystals," Nat. Photonics **2**(8), 465–473 (2008).
11. M. Soljačić, S. G. Johnson, S. H. Fan, M. Ibanescu, E. Ippen, and J. D. Joannopoulos, "Photonic-crystal slow-light enhancement of nonlinear phase sensitivity," J. Opt. Soc. Am. B **19**(9), 2052–2059 (2002).
12. S. A. Schulz, L. O'Faolain, D. M. Beggs, T. P. White, A. Melloni, and T. F. Krauss, "Dispersion engineered slow light in photonic crystals: a comparison," J. Opt. **12**(10), 104004 (2010).
13. B. Corcoran, M. D. Pelusi, C. Monat, J. Li, L. O'Faolain, T. F. Krauss, and B. J. Eggleton, "Ultracompact 160 Gbaud all-optical demultiplexing exploiting slow light in an engineered silicon photonic crystal waveguide," Opt. Lett. **36**(9), 1728–1730 (2011).

#165348 - $15.00 USD Received 26 Mar 2012; revised 17 May 2012; accepted 29 May 2012; published 2 Jul 2012

14. R. J. P. Engelen, Y. Sugimoto, Y. Watanabe, J. P. Korterik, N. Ikeda, N. F. van Hulst, K. Asakawa, and L. Kuipers, "The effect of higher-order dispersion on slow light propagation in photonic crystal waveguides," Opt. Express **14**(4), 1658–1672 (2006).
15. L. C. Andreani and D. Gerace, "Light-matter interaction in photonic crystal slabs," Phys. Status Solidi B **244**(10), 3528–3539 (2007).
16. T. F. Krauss, "Why do we need slow light?" Nat. Photonics **2**(8), 448–450 (2008).
17. C. Monat, M. de Sterke, and B. J. Eggleton, "Slow light enhanced nonlinear optics in periodic structures," J. Opt. **12**(10), 104003 (2010).
18. T. F. Krauss, "Slow light in photonic crystal waveguides," J. Phys. D Appl. Phys. **40**(9), 2666–2670 (2007).
19. C. Monat, B. Corcoran, M. Ebnali-Heidari, C. Grillet, B. J. Eggleton, T. P. White, L. O'Faolain, and T. F. Krauss, "Slow light enhancement of nonlinear effects in silicon engineered photonic crystal waveguides," Opt. Express **17**(4), 2944–2953 (2009).
20. S. Combrié, Q. V. Tran, A. de Rossi, C. Husko, and P. Colman, "High quality GaInP nonlinear photonic crystals with minimized nonlinear absorption," Appl. Phys. Lett. **95**(22), 221108 (2009).
21. V. Eckhouse, I. Cestier, G. Eisenstein, S. Combrié, P. Colman, A. De Rossi, M. Santagiustina, C. G. Someda, and G. Vadalà, "Highly efficient four wave mixing in GaInP photonic crystal waveguides," Opt. Lett. **35**(9), 1440–1442 (2010).
22. M. Santagiustina, C. G. Someda, G. Vadalà, S. Combrié, and A. De Rossi, "Theory of slow light enhanced four-wave mixing in photonic crystal waveguides," Opt. Express **18**(20), 21024–21029 (2010).
23. S. Combrié, Q. V. Tran, E. Weidner, A. de Rossi, S. Cassette, P. Hamel, Y. Jaouen, R. Gabet, and A. Talneau, "Investigation of group delay, loss and disorder in a photonic crystal waveguide by low-coherence reflectometry," Appl. Phys. Lett. **90**(23), 231104 (2007).
24. P. Colman, S. Combrié, G. Lehoucq, and A. De Rossi, "Control of dispersion in photonic crystal waveguides using group symmetry theory," Opt. Express **20**(12), 13108–13114 (2012).
25. Q. V. Tran, S. Combrié, P. Colman, and A. De Rossi, "Photonic crystal membrane waveguides with low insertion losses," Appl. Phys. Lett. **95**(6), 061105 (2009).
26. M. Patterson, S. Hughes, S. Combrié, N. V. Tran, A. De Rossi, R. Gabet, and Y. Jaouën, "Disorder-induced coherent scattering in slow-light photonic crystal waveguides," Phys. Rev. Lett. **102**(25), 253903 (2009).
27. S. Hughes, L. Ramunno, J. F. Young, and J. E. Sipe, "Extrinsic optical scattering loss in photonic crystal waveguides: role of fabrication disorder and photon group velocity," Phys. Rev. Lett. **94**(3), 033903 (2005).
28. L. O'Faolain, T. P. White, D. O'Brien, X. Yuan, M. D. Settle, and T. F. Krauss, "Dependence of extrinsic loss on group velocity in photonic crystal waveguides," Opt. Express **15**(20), 13129–13138 (2007).
29. E. Kuramochi, M. Notomi, S. Hughes, A. Shinya, T. Watanabe, and L. Ramunno, "Disorder-induced scattering loss of line defect waveguides in photonic crystal slabs," Phys. Rev. Lett. B. **72**(16), 161318 (2005).
30. C. Husko, S. Combrié, Q. V. Tran, F. Raineri, C. W. Wong, and A. De Rossi, "Nontrivial scaling of self-phase modulation and three-photon absorption in III-V photonic crystal waveguides," Opt. Express **17**(25), 22442–22451 (2009).
31. C. Husko, P. Colman, S. Combrié, A. De Rossi, and C. W. Wong, "Effect of multiphoton absorption and free carriers in slow-light photonic crystal waveguides," Opt. Lett. **36**(12), 2239–2241 (2011).
32. K. Lengle, A. Akrout, M. Costa e Silva, L. Bramerie, J. C. Simon, S. Combrie, P. Colman, and A. de Rossi, "10 GHz demonstration of four wave mixing in photonic crystal waveguides," in *2010 36th European Conference and Exhibition on Optical Communication (ECOC)* (2010), paper P2.24.
33. M. Ebnali-Heidari, C. Monat, C. Grillet, and M. K. Moravvej-Farshi, "A proposal for enhancing four-wave mixing in slow light engineered photonic crystal waveguides and its application to optical regeneration," Opt. Express **17**(20), 18340–18353 (2009).
34. M. R. Lamont, B. T. Kuhlmey, and C. M. de Sterke, "Multi-order dispersion engineering for optimal four-wave mixing," Opt. Express **16**(10), 7551–7563 (2008).
35. M. A. Foster, A. C. Turner, R. Salem, M. Lipson, and A. L. Gaeta, "Broad-band continuous-wave parametric wavelength conversion in silicon nanowaveguides," Opt. Express **15**(20), 12949–12958 (2007).
36. P. Colman, I. Cestier, A. Willinger, S. Combrié, G. Lehoucq, G. Eisenstein, and A. De Rossi, "Observation of parametric gain due to four-wave mixing in dispersion engineered GaInP photonic crystal waveguides," Opt. Lett. **36**(14), 2629–2631 (2011).
37. I. Cestier, A. Willinger, P. Colman, S. Combrié, G. Lehoucq, A. De Rossi, and G. Eisenstein, "Efficient parametric interactions in a low loss GaInP photonic crystal waveguide," Opt. Lett. **36**(19), 3936–3938 (2011).
38. S. Mazoyer, A. Baron, J. P. Hugonin, P. Lalanne, and A. Melloni, "Slow pulses in disorder photonic-crystal waveguides," Appl. Opt. **50**(31), G113–G117 (2011).

1. Introduction

In the context of a growing need for high-speed transmissions with at the same time the will of reducing energy consumption in telecommunications networks, data-signal processing at the optical level can help significantly to achieve these goals, leading to a simplification of the future telecommunication networks.

#165348 - $15.00 USD Received 26 Mar 2012; revised 17 May 2012; accepted 29 May 2012; published 2 Jul 2012

Over the last years there has been a growing interest on photonic crystals (PhC) to perform optical functions, such as pulse compression [1], all-optical storage [2,3] and all-optical switching [4] owing to their small footprint and high nonlinearity. The reduced effective mode area in PhC waveguide is indeed of particular interest to enhance nonlinearities and recently allowed the observation of optical solitons [1]. Nonlinearity exacerbation has been demonstrated so far in high-index materials, such as Silicon [5–7] and III-V semiconductors [8,9]. Moreover PhC waveguides provide the possibility to engineer the dispersion and the group index [10–19] through the careful design of the waveguide so that the phase matching of the four wave mixing (FWM) process is optimized. Slow light in photonic crystals thus open the possibility to fabricate compact optical functions [10,13,16]. Investigation of the role of group velocity on FWM process has indeed been carried out on Silicon PhC waveguides [6,7,12,13]. In the same time, PhC waveguides based on two-photon absorption (TPA)-free materials, enabling efficient nonlinearity at high optical power propagation, have recently been conceived [20] and studied [21,22].

In this paper, we present the first deep experimental study of the benefit of dispersion-engineered in GaInP PhC waveguides for FWM generation. Two self-standing membrane, single line defect waveguides are compared. Both structures have a triangular lattice of holes with the same parameters but the second one is dispersion-engineered by the anti-symmetric translation of the first rows closest to the core, in order to enhance the group index and control the dispersion. Experimental FWM efficiency maps (as a function of pump wavelength and spectral detuning dependence) are investigated for the first time in two GaInP PhC waveguides with different design. Additionally, time-resolved measurements with short pulses at 10 GHz and transmission of a RZ 40 Gbit/s signal are carried out in our waveguides.

This paper is organized as follow: section 2 gives a brief description of our photonic crystal waveguides. Section 3 describes FWM time-resolved experiments and gives a comparison of this effect through the study of experimental FWM efficiency maps. The negligible impact of slow-light on transmission perturbations on a RZ 40 Gbit/s signal is finally discussed in section 4.

2. Photonic crystal waveguides

2.1 Self-standing membrane structure

Two PhC devices are studied in this paper; both are self-standing membrane structures with a 170 nm thick slab of GaInP patterned with a triangular lattice (period a = 480 nm) of holes with radii r = 0.19 a. The 1.3 mm long waveguide results from the omission of a single row of holes in the 2D lattice of holes structure as it can be seen on the SEM pictures of Figs. 1(a) and 1(b). This allows the propagation of a mode within the photonic bandgap. This material is TPA-free in the telecom spectral band, in contrast to Si [13], or in GaAs PhC. Indeed, the electronic bandgap of GaInP (E_g ~1.9 eV) is greater than twice the energy of photons in the telecom band (~0.8 eV), thereby preventing from TPA.

The first structure is the one describe above and will be referred as the ‘low group index’ device and the second has been designed in order to enhance the group index and control the

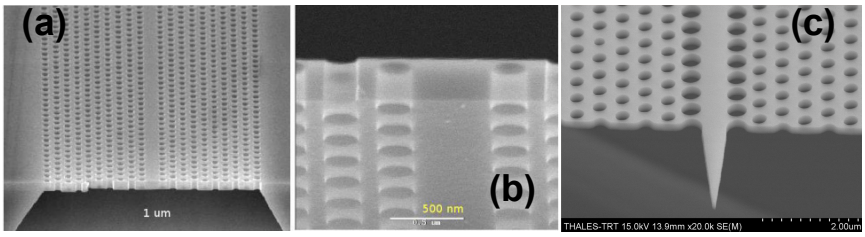

Fig. 1. PhC waveguide SEM pictures: self-standing membrane with triangular lattice of holes (a-b), mode adapting structure (c) (source: Thales TRT).

#165348 - $15.00 USD Received 26 Mar 2012; revised 17 May 2012; accepted 29 May 2012; published 2 Jul 2012

dispersion. The technique is based on an asymmetric translation of the holes rows closest to the core as explained in [23,24]. Physical parameters are the same as in the first component except the first rows which are anti-symmetrically translated by a value $T = 0{,}1 \times a$ as described in [24].

Mode adapting structures were developed to minimize optical coupling losses and to suppress Fabry-Perot oscillations as shown in Fig. 1(c). More details of the technology can be found in [20,25].

2.2 Group index, dispersion parameter and transmission curves

The interferometric technique of [23] was used to measure the group index (continuous line), which is shown in Figs. 2(a) and 2(b) for the 'low group index' and 'dispersion engineered' devices respectively. The dispersion parameter β_2 was extracted from numerical derivative functions calculations of the group index (dashed line).

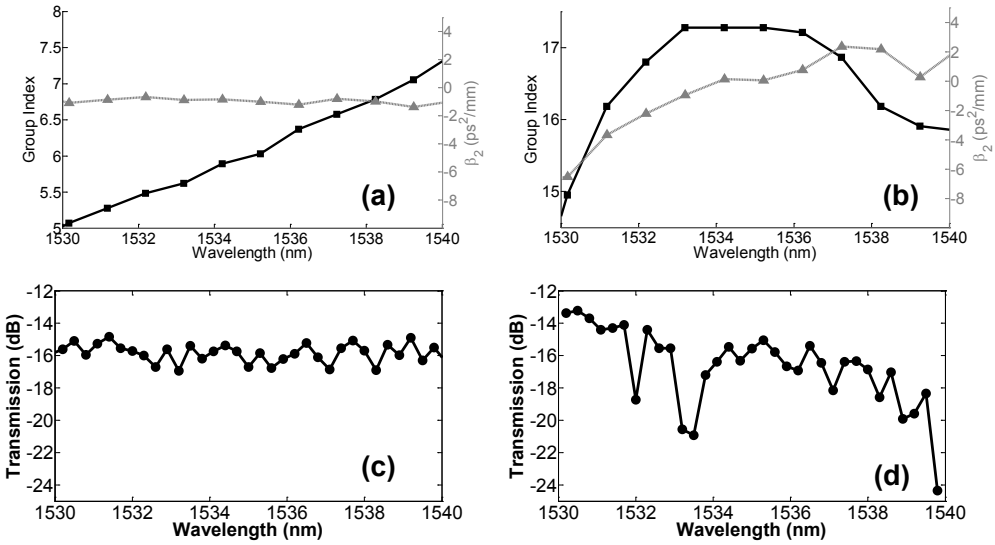

Fig. 2. (a, b) Group index profiles (continuous line, squares) and GVD profiles (dotted line, triangles) of the tested waveguides, with associated transmission profiles (c, d).

The transmission of the 'low group index' device is plotted in Fig. 2(c). For this waveguide, the group index ranges between 5 and 7.5 with a fiber-to-fiber losses for TE mode around 16 dB in the spectral range considered here (1530 nm-1540 nm). The dispersion parameter is rather constant and around −1 ps^2/mm, which is quite high actually as it corresponds to a dispersion parameter $D \sim 785 \times 10^3$ ps/nm.km.

The transmission of the 'dispersion-engineered' device is plotted in Fig. 2(d). The maximum group index reached here is larger (n_g = 17) and an almost flat band is obtained over 4 nm. It should be stressed that in our study, we do not try to reach a higher group index but a trade-off on design between nonlinearity and transmission losses. Between 1533 and 1537 nm, the dispersion parameter varies between –1 and + 1 ps^2/mm. On this flat band, β_2 is null on only 1 nm bandwidth consequently the flat band where we can expect a non-linear enhancement linked to slow-light regime will be also reduced. Moreover, on Fig. 2(d) we can see a transmission with more perturbations and with excess losses in the flat band slow light as expected by lattice imperfections which are more critical in the slow light regime [26] leading to an enhancement of linear [27–29] and nonlinear [30,31] propagation losses. Transmission losses also increase with increasing wavelength when approaching the forbidden band gap frequency.

#165348 - $15.00 USD Received 26 Mar 2012; revised 17 May 2012; accepted 29 May 2012; published 2 Jul 2012

A highest FWM efficiency has been demonstrated in slow-light PhC waveguides [6,7]; in our case, due to longer waveguide (1.3 mm) and non-negligible group velocity dispersion (GVD) in the flat band group index range, the slow light benefit is less obvious. We thus compare the FWM efficiency in the dispersion-engineered waveguide with our low group index waveguide. Moreover, it is the first comparison in III-V material.

3. Four wave mixing

3.1 Time-resolved measurements

In the degenerate FWM configuration considered here, a single pump, at a frequency ω_{pump} and wavevector k_{pump} is mixed with a probe signal at a frequency ω_{probe} and wavevector k_{probe}. While the probe is amplified through the FWM process, an idler signal, at a frequency ω_{idler} and wavevector k_{idler}, is simultaneously generated, as inferred from the expression of the nonlinear polarization P_{NL} at the idler frequency:

$$P_{NL} = \frac{3}{2}\varepsilon_0 \chi^{(3)} E_{pump}^2 E_{probe}^* e^{i(\Delta k_L - \Delta\omega t)} \tag{1}$$

where ε_0 is the free space permittivity, and E_{pump} and E_{probe} are the pump and probe input electric field amplitudes that overlap in time. The frequency and wave vector differences respectively are given by the following equations:

$$\Delta\omega = 2\omega_{pump} - \omega_{probe} - \omega_{idler} \tag{2}$$

$$\Delta k_L = 2k_{pump} - k_{probe} - k_{idler} \tag{3}$$

In a first experiment, we observed the generation of the idler signal thanks to a time-resolved measurement based on optical gating (optical sampling oscilloscope, OSO) with a time resolution of 1 ps. This experiment is performed on the low group index propagation regime waveguide and aims at observing if the converted signal undergoes some time deformations.

The experimental setup is presented on Fig. 3. We used a pulsed pump signal at a repetition rate of 10 GHz with 5 ps pulses and a continuous wave (CW) probe signal. Both signals polarizations are controlled before coupling together to ensure both signals to be co–polarized on TE mode. Figure 4(a) shows the transmission spectra at the PhC output, as a function of the pump-probe detuning. The FWM idler and CW probe appear as symmetrical pairs as the detuning is changed. The FWM signal disappears when the probe is off (black trace on Fig. 4(a)). We can notice cross phase modulation (XPM) induced by the pump on the

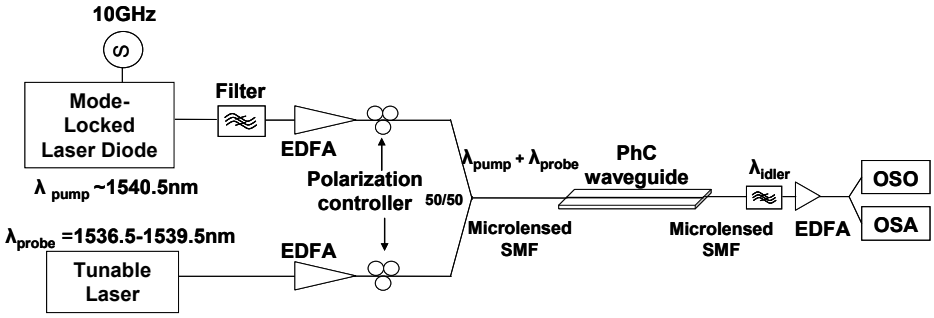

Fig. 3. Experimental setup for time response limitation investigation.

#165348 - $15.00 USD Received 26 Mar 2012; revised 17 May 2012; accepted 29 May 2012; published 2 Jul 2012

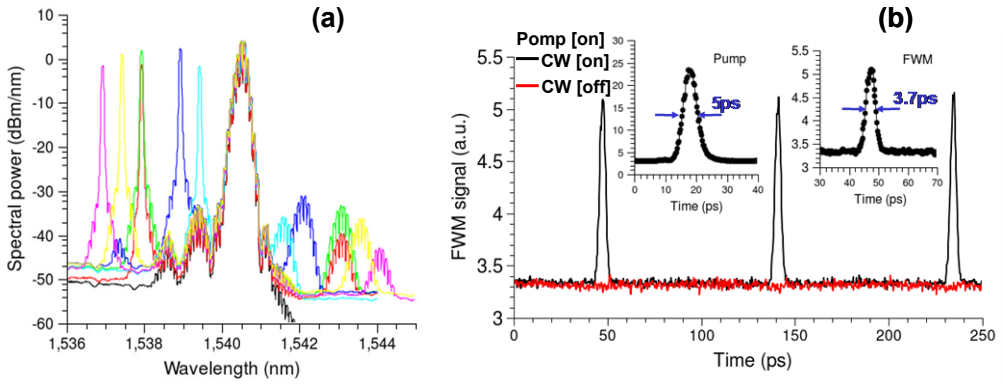

Fig. 4. FWM in a "low group index" PhC waveguide. (a) transmitted spectra; colors are related to the pump-probe detuning, the black curve represents the output without CW signal and (b) Time-resolved traces using an optical sampling oscilloscope.

CW probe since 10 GHz modulation lines appear on the probe signal. We can also notice some side lobes on the pump signal which come from the mode-locked laser used as a pulsed source.

For the time response measurement, a filter is placed at the output and centered on the idler signal in order to filter out pump and probe light. Figure 4(b) shows temporal traces when the probe is off (red trace) and on (black trace) with a pump mean power before coupling of 18 dBm, a probe power of 13 dBm and a spectral detuning of −2 nm, which is defined as the difference between the probe and the pump wavelengths of Eq. (4):

$$\Delta\lambda = \lambda_{probe} - \lambda_{pump} \tag{4}$$

First, we show that when pump is on and the probe is off, the FWM signal is zero, which is consistent with the black curve in Fig. 4(a), and corresponds to the optical noise of the last optical amplifier. This supports the claim that the pump is effectively filtered out and does not reach the optical sampling oscilloscope. Now, when both pump and probe are on, the FWM idler signal appears and the converted pulse is quite short. The inset shows a close up of the pump and the idler temporal traces. It should be noted that the converted pulse is slightly shorter (3.7 ps) and matches the profile of the input pulse (5 ps) squared (e.g. E(idler) $\propto$ E(pump)^2), exactly as the theory of ultra-fast parametric conversion predicts [32].

This implies that the response is of pure Kerr origin, hence ultra-fast. In addition, the inspection of the traces does not reveal any distortion that could arise from free carrier generation. Limitations due to carrier recombination time are not expected, even at high data rate. Indeed, no evidence of patterning or thermal effects has emerged from our measurements at 10 GHz. Moreover, it should be noted that the demonstration of faster data rate was prevented by the availability of an appropriate laser source at the time of the experiment.

3.2 Experimental setup for FWM efficiency maps

Here we report a comparison between the low group index and the dispersion-engineered waveguides. The experimental set-up (Fig. 5) was modified in order to improve the wavelength flexibility and the peak power. The pump and probe are synchronized 100 ps pulses generated by two continuous wave lasers modulated with a Mach-Zehnder modulator driven by a pattern generator at 10 Gbit/s generating words of one bit '1' followed by 19 bits '0' allowing to reduce the repetition rate down to 500 MHz with 100 ps pulses, so the peak power increases at constant mean power. Both signals are then amplified and polarized so as

#165348 - $15.00 USD Received 26 Mar 2012; revised 17 May 2012; accepted 29 May 2012; published 2 Jul 2012

to excite the TE mode. An optical filter with a 5 nm bandwidth was used to remove the spontaneous emission originating from the EDFAs.

Finally, the signals are coupled into the PhC waveguide with a microlensed fiber providing a focused spot of 2 μm at $1/e^2$ intensity. The transmitted light is collected with a second microlensed fiber and analyzed using an optical spectrum analyzer. Before coupling, the pump and probe average power are about 16 dBm and 13 dBm respectively.

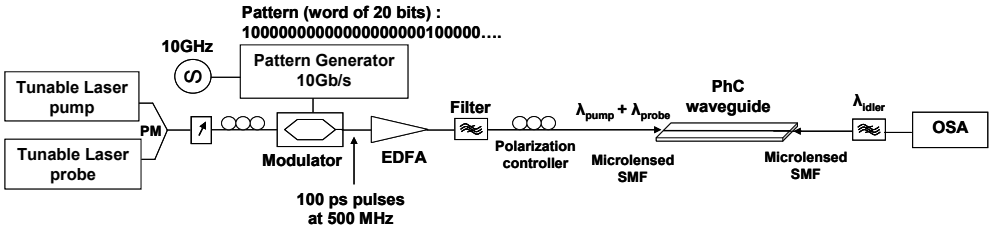

Fig. 5. Experimental setup for FWM map characterization with 100 ps pulses at 500 MHz.

3.3 FWM enhancement in dispersion engineered PhC waveguides

The FWM efficiency is defined by the ratio of Eq. (5):

$$\eta_{FWM} \equiv \frac{\overline{P_{idler}}(out)}{\overline{P_{probe}}(in)} \tag{5}$$

With $\overline{P_{idler}}(out)$ and $\overline{P_{probe}}(in)$ respectively the mean powers of the output idler signal and the input probe signal.

It should be noted that, in the literature, several definitions of FWM efficiency are used. When both pump and probe signals are pulsed and with the same duty cycle, the definition of the ratio of mean powers of the output idler signal to the input probe signal (Eq. (5)) can be used. Let us notice that this definition includes device insertion losses as the user point of view is considered so that "fiber-PhC waveguide-fiber" is considered as a whole. This is not always the case in the literature (when output probe signal is considered in the definition); knowing that insertion losses are superior to 15 dB in the device, it makes a big difference in the FWM efficiency calculation when losses are not considered; this remark shows that FWM efficiency records reported in the literature is relative to the used definition.

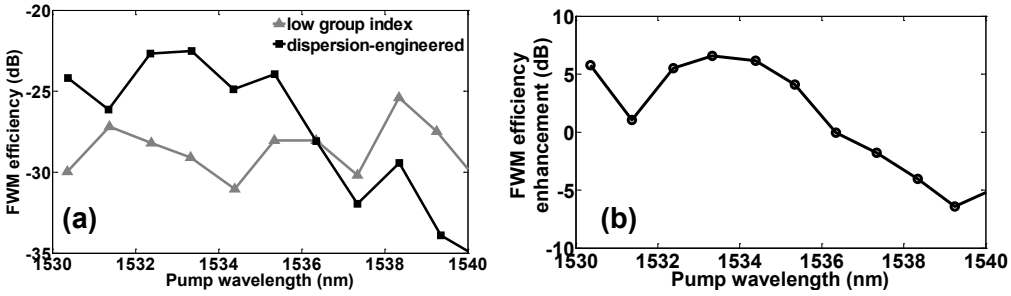

Fig. 6. (a) FWM efficiencies for 'low group index' (gray curve) and dispersion-engineered (black curve) waveguides as a function of pump wavelength when the pump-probe detuning is 0.65 nm; (b) FWM efficiency enhancement between both devices as a function of pump wavelength.

In Fig. 6(a), we plot FWM efficiency as a function of the pump wavelength when the pump-probe detuning is 0.65 nm which corresponds to the smaller pump-probe detuning we can achieve in our setup and which corresponds to the highest efficiency we can obtain.

#165348 - $15.00 USD Received 26 Mar 2012; revised 17 May 2012; accepted 29 May 2012; published 2 Jul 2012

Based on that, we estimated the optimal pump wavelength providing the largest conversion efficiency, as in our waveguides, the pump wavelength is a key parameter as the GVD is not flat on the working wavelength range. The largest conversion efficiency of −25.5 dB is obtained at 1538.3 nm for the low group index waveguide and of −22.2 dB at 1533.8 nm for the dispersion-engineered waveguide.

In Fig. 6(b), we plot the FWM efficiency enhancement between both devices as a function of the pump wavelength. At 1530 nm and 1532 nm we measure an enhancement of 5.8 dB in the FWM efficiency. This difference can be explained by the higher group index and the lower fiber-to-fiber losses in the dispersion engineered waveguide. From 1532 nm to 1535 nm the losses are identical in two waveguides (around 16 dB) and the FWM efficiency enhancement reaches a maximum of 6.9 dB at 1533.8 nm. This wavelength corresponds to a high group index and a slight negative GVD in the dispersion engineered waveguide which demonstrates that the enhancement is due to slow-light regime. At pump wavelength higher than 1535 nm, the FWM efficiency enhancement decreases due to increasing losses and positive GVD which increases the linear phase mismatch.

The enhancement of the nonlinear response is related to the so-called "slow down factor" S, which is defined by Eq. (6) as the ratio of the phase velocity v_φ to the group velocity v_g, or equivalently as the refractive index ratio of the group index n_g to the phase index n_0 [16]:

$$S = \frac{v_\varphi}{v_g} \Rightarrow S = \frac{n_g}{n_0} \tag{6}$$

It has been shown that FWM scales as the fourth power of the slowdown factor (namely $\eta \propto S^4$) in slow-light regime [6]. Therefore, if two waveguides bear the same losses, but the dispersion-engineered sample is operated at a 3-fold larger group index, a FWM efficiency enhancement of 19 dB would be expected. However, an enhancement of only about 7 dB is expected, namely 12 dB below the prediction, which assumes a flat dispersion (negligible GVD) in the waveguide. As this is not yet the case, pulse broadening and temporal walk-off occur. More importantly, the FWM process is not phase-matched, thereby reducing the efficiency. More precisely, the dispersion is approximately flat only over a bandwidth of 1 nm. Since the smallest pump-probe possible detuning in our experiment is 0.65 nm, the pump, probe and idler cannot all fit in the tiny "flat-band". In addition, a 5 dB increase of losses appear around 1533.5 nm on the dispersion engineered device, which further reduces the FWM efficiency.

This said, the overall efficiency is still very good (−22 dB with high repetition rate signals) because the waveguide is much longer 1.3 mm than what is used elsewhere [6,7,12,13].

The FWM efficiency curves were then extended to FWM efficiency maps by tuning both the pump wavelength and the pump-probe detuning.

3.4 FWM efficiency maps

FWM efficiency maps are plotted in Fig. 7 for both waveguides. The pump-probe detuning range is 3.6 nm, with 0.3 nm steps, while pump wavelength ranges from 1530 nm to 1540 nm, with a 1 nm step.

The first observation is that with the 'low group index' device, the map is quite monotonous with a similar behavior whatever the pump wavelength and the spectral detuning is. On the contrary, with the 'dispersion-engineered' device, 3 areas can be observed: an area where the FWM is efficient on a larger spectral detuning (slightly below 1536 nm), an area with a very low FWM efficiency (for a pump wavelength larger than 1536 nm) and an area with a decreasing spectral detuning for a given FWM efficiency (for a pump wavelength smaller than 1536 nm).

#165348 - $15.00 USD Received 26 Mar 2012; revised 17 May 2012; accepted 29 May 2012; published 2 Jul 2012

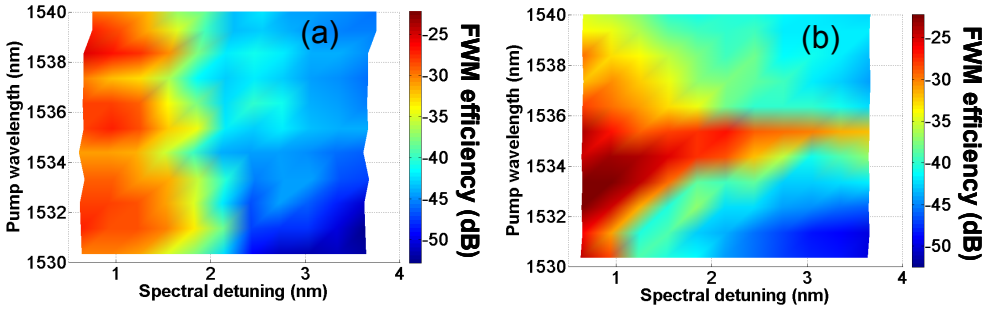

Fig. 7. FWM efficiency map for 'low group index' (a) and for dispersion-engineered (b) waveguides

We will introduce a number of definitions in order to analyze this behavior differences. The measured FWM conversion efficiency has been written in [33] as

$$\eta_{FWM} = \frac{\overline{P_{idler}}(out)}{\overline{P_{probe}}(in)} = \left(\frac{\gamma \overline{P_{pump}}}{g} \sin \mathrm{h}(gL) \right)^2 e^{-\alpha L} \tag{7}$$

The waveguide length is L and γ is self-phase modulation coefficient for the waveguide. $\overline{P_{pump}}$ is the path average pump power, corrected by accounting for the propagation loss α.

The parametric gain g, determines how the idler power evolves along the propagation distance. It is defined by Eq. (8):

$$g = \sqrt{\left(\gamma \overline{P_{pump}}\right)^2 - \left(\frac{\Delta k}{2}\right)^2} \tag{8}$$

The parametric gain will thus increase with a better phase matching. The net phase mismatch Δk, as given in Eq. (9), is the sum of the linear phase mismatch Δk_L and a nonlinear contribution Δk_{NL}, arising from cross phase modulation (XPM) and self-phase modulation (SPM):

$$\Delta k = \Delta k_L + \Delta k_{NL} \tag{9}$$

Thus, in order to maximize the FWM efficiency, a negative linear phase mismatch is required in order to offset the nonlinear contribution. The linear phase mismatch, of Eq. (9) can be approximated as follows in Eq. (10). We can see the dependence on second and fourth orders of dispersion parameters (only odd orders because degenerate FWM is considered):

$$\Delta k_L \approx (\Delta \omega)^2 \beta_2 + \frac{1}{12} (\Delta \omega)^4 \beta_4 \tag{10}$$

It has been theoretically demonstrated [33,34], in high refractive index materials, that a low negative second order dispersion is required in order to maximize the net phase matching and so increase the FWM efficiency.

Now, the FWM conversion bandwidth Ω_{FWM} is the maximum pump and probe detuning for which $|\Delta k.L| < \pi$ and is slightly larger than the 3 dB bandwidth which is experimentally measured. In the small-gain limit ($2\gamma P_{pump} L < \pi$), the conversion bandwidth is independent of the pump power, and is defined by [35]

$$\Omega_{FWM} \approx \sqrt{\frac{4\pi}{|\beta_2| L}} \tag{11}$$

#165348 - $15.00 USD Received 26 Mar 2012; revised 17 May 2012; accepted 29 May 2012; published 2 Jul 2012

Equation (11) leads to a spectral detuning defined by Eq. (12):

$$\Delta\lambda \approx \Omega_{FWM} \cdot \frac{\lambda^2}{2\pi c} \tag{12}$$

This equation shows that same conditions are required on β_2 in order to increase the FWM conversion bandwidth. Let us notice that we do not focus here on the fourth order dispersion parameter that does not have an impact on FWM efficiency but does have one on the conversion bandwidth [34].

Let us now focus on the FWM efficiency maps and compare them with what is expected from the theory. In the case of the low group index waveguide in Fig. 7(a), for a given spectral detuning the FWM efficiency is almost constant in the considered pump wavelength range and typically varies between −25.5 dB and −28 dB for a spectral detuning of 0.65 nm. In this range β_2 is constant and negative (about −1 ps^2/mm) (Fig. 2(a)). As shown by equations above, this leads to a constant linear phase mismatch and thus to a constant parametric gain and FWM efficiency.

The FWM conversion bandwidth is approximately constant over all the considered pump wavelength range and is about 1.6 nm. Considering Eq. (10) and a GVD ~-1 ps^2/mm, the conversion bandwidth should be theoretically a bit less than 4 nm which is not too far from our experimental result considering the fact that the conversion bandwidth definition is larger from the 3 dB conversion bandwidth [35].

Now, in the case of the dispersion-engineered waveguide (Fig. 7(b)), three regions can be considered in the map: in the first region (the pump wavelength is slightly below 1536 nm), the conversion bandwidth is the largest (~2 nm) and corresponds to the area where the GVD sign changes, as expected. However, the actual value of the FWM bandwidth does not follow Eq. (10) strictly, as here the GVD is approximately zero only over a spectral span of 1 nm. In the second region (defined by pump wavelength being larger than 1536 nm), the FWM efficiency decreases (below −30 dB), as β_2 is positive and large (hence larger phase mismatch); here the conversion bandwidth decreases as well. In the third region (pump wavelength shorter than 1536 nm), the FWM efficiency stays relatively high at small spectral detuning (~-26 dB) but the conversion bandwidth decreases. In this area β_2 is negative, compensating for the nonlinear phase mismatch and $|\beta_2|$ increases.

The visual comparison of the two maps makes apparent the role of dispersion in the FWM process.

It should be noted that, while the maximum group index achieved here is not as large as reported by other groups [13], here our TPA free material allows longer waveguides (1.3 mm) leading to comparable efficiency. Indeed, in the same waveguide we have reported gain for the first time in PhCs [36,37]. Let us notice that pump signals are not the same in both papers leading to different power ranges: in [36] coupled peak power is about 4 W, whereas it is about 250 mW in this work as the pulses are much longer; the gain regime can thus not be reached with such long pulses.

Despite the potential benefits of dispersion engineering, the design of the sample considered here needs further optimization in order to achieve a more efficient wavelength conversion and make it strongly attractive for telecom applications. Indeed, for 40 Gbit/s or 160 Gbit/s signals, the FWM bandwidth is limited.

4. 40 Gbit/s linear propagation

It is now well known that fabrication imperfections in PhCs result into backscattering [27] or even multiple scattering [26], which could be detrimental for the propagation of data signals. In addition these effects are critically dependent on the group velocity. In the last part of this

#165348 - $15.00 USD Received 26 Mar 2012; revised 17 May 2012; accepted 29 May 2012; published 2 Jul 2012

paper, we have therefore evaluated the impact of these effects on the quality of transmitted signals specifically 40 Gbit/s Return to Zero.

The measurement is carried out on a dispersion-engineered waveguide at two wavelengths corresponding to different values of the group velocity and dispersion, as shown in Fig. 8. Left side shows input and output spectra (res. 0.07nm) and the fiber-to-fiber transmission (res. 0.01nm) for both regimes. As expected in [38], when entering into the "slow-light" regime, perturbations of the transmission spectra are more marked, indeed disorder manifests as an increasingly irregular transmission as the group index increases. It leads to spectral deformations.

In order to provide a measurement of the impact of fabrication imperfections, we perform the bit error rate (BER) analysis with the related eye diagrams (Fig. 9) at 11 dBm before coupling. Moreover it is to notice that results are similar up to the power range which is used for FWM experiments, i.e. ~16 dBm before coupling. We performed error free operation in both regimes. At BER of 10^{-9}, we measure no penalty when the group index is relatively low whereas there is a 1 dB penalty in the slow light propagation regime. We attribute this to the

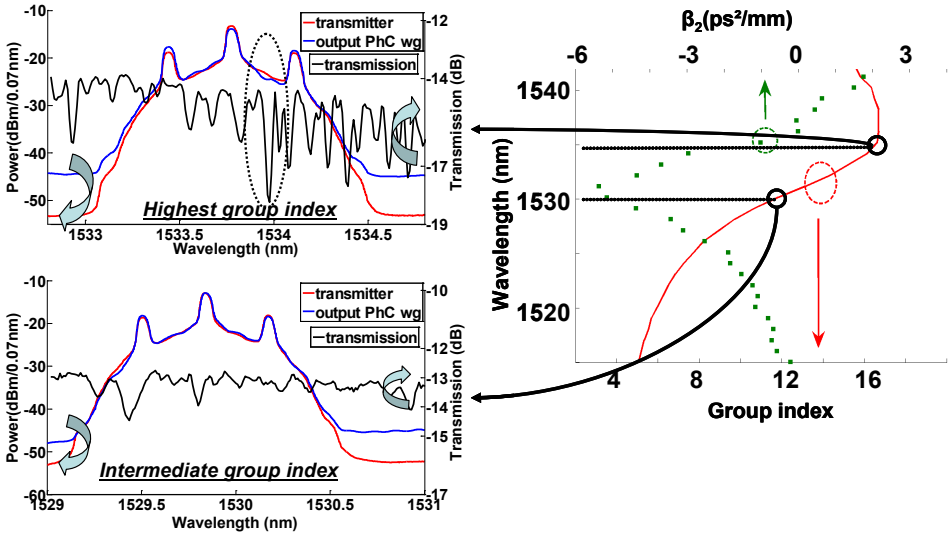

Fig. 8. Fiber to fiber transmission and input / output spectra in both propagation regimes, linked to group index profile of the waveguide.

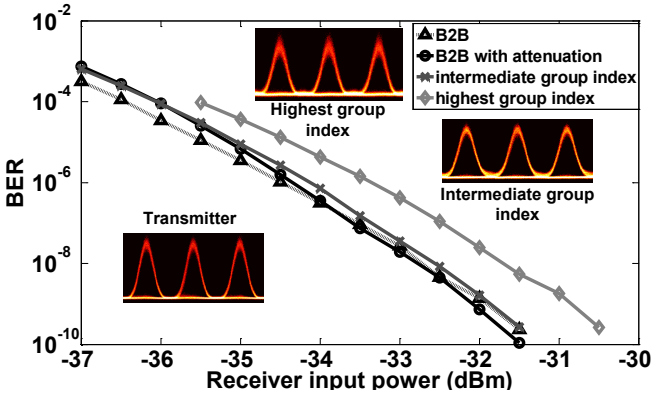

Fig. 9. Bit error rate measurements of 40 Gbit/s RZ signal transmission through PhC waveguide with associated eye diagrams.

#165348 - $15.00 USD Received 26 Mar 2012; revised 17 May 2012; accepted 29 May 2012; published 2 Jul 2012

distortion of the transmission spectra as shown in Fig. 8. However, this impact is moderate, thereby allowing assessment of the device for the transmission of telecom signals at high bit rates.

5. Conclusion

We have compared the single missing line defect photonic crystal waveguide with a novel design implementing dispersion-engineered using Gallium Indium Phosphide as nonlinear material. The benefit of GaInP is the much reduced nonlinear absorption, as compared to Silicon. We have demonstrated Four Wave Mixing conversion efficiency as large as –22 dB, including coupling losses. We show that our dispersion-engineered waveguides feature a larger (~7dB) conversion efficiency, compared to the single missing line defect design. We report FWM efficiency maps, which clearly highlight the different response of the two structures. However, the present design suffers from a limited usable bandwidth. Further effort will be devoted to improve the conversion bandwidth in order to implement practical nonlinear functions. We also demonstrate the absence of any carrier-related impairment, by time-resolved measurements with short pulses at 10 GHz. We also show that the residual modulation of the transmission due to disorder-induced scattering has little impact over the transmission of data signal, was the BER measured on a RZ signal at 40 Gbit/s transmitted through the waveguide demonstrated almost error free operation (1 dB penalty at a BER of 10^{-9}).

Acknowledgments

We acknowledge support by the EU through the Copernicus project (249012) (www.copernicusproject.eu). This work was also supported by Region Bretagne.

#165348 - $15.00 USD Received 26 Mar 2012; revised 17 May 2012; accepted 29 May 2012; published 2 Jul 2012